

Geometry-informed Channel Statistics Prediction Based upon Uncalibrated Digital Twins

Mahmoud Saad Abouamer[†], Robin J. Williams^{*}, Petar Popovski^{*}

^{*}Department of Electronic Systems, Aalborg University, Denmark

[†]Department of Electrical and Computer Engineering, University of Waterloo, Canada
email: mabouamer@uwaterloo.ca, rjw@es.aau.dk, petarp@es.aau.dk

Abstract—Digital twins (DTs) of wireless environments can be utilized to predict the propagation channel and reduce the overhead of required to estimate the channel statistics. However, direct channel prediction requires data-intensive calibration of the DT to capture the environment properties relevant for propagation of electromagnetic signals. We introduce a framework that starts from a satellite image of the environment to produce an *uncalibrated* DT, which has no or imprecise information about the materials and their electromagnetic properties. The key idea is to use the uncalibrated DT to implicitly provide a geometric prior for the environment. This is utilized to inform a Gaussian process (GP), which permits the use of few channel measurements to attain an accurate prediction of the channel statistics. Additionally, the framework is able to quantify the uncertainty in channel statistics prediction and select rate in ultra-reliable low-latency communication (URLLC) that complies with statistical guarantees. The efficacy of the proposed geometry-informed GP is validated using experimental data obtained through a measurement campaign. Furthermore, the proposed prediction framework is shown to provide significant improvements compared to the benchmarks where i) direct channel statistics prediction is obtained using an uncalibrated DT and (ii) the GP predicts channel statistics using information about the location.

Index Terms—Digital twin, channel statistics map, Gaussian process, ultra reliable low latency communications, rate selection.

I. INTRODUCTION

Digital twins (DTs) that accurately model wireless channels have demonstrated significant utility for both communication and localization tasks [1]. For instance, by maintaining a precise DT, site-specific digital twins can be used to reduce CSI acquisition and feedback overhead [2]. Additionally, DT-generated fingerprinting databases be used to improve positioning accuracy [3]. However, for the DT to provide accurate predictions, its electromagnetic properties should match real-world channel conditions. The process of configuring the objects and materials in the DT to represent the wireless environment is referred to as *calibration*.

Differentiable ray tracers (RT), such as Sionna RT [4] are instrumental in enabling effective calibration methods. Differentiable RTs allow the computation of gradients for

system parameters, enabling tasks like data-driven material property optimization. This was demonstrated in recent works, such as [5, 6], which leverage differentiable RT for material optimization. For instance, to address phase errors caused by geometric discrepancies, [6] employs a variational expectation maximization algorithm for mitigating phase errors and thereby improving prediction accuracy.

This work treats the problem of resource allocation for ultra reliable low latency communications. The problem is to pick a data-rate which satisfies a set of reliability and latency constraints. Due to the latency constraint, channel feedback procedures are not always feasible. In such cases, the system must rely on alternatives such as channel statistics maps to select a rate which satisfies the reliability constraint with a sufficiently high probability. Indeed, a fully calibrated DT which accurately represents the objects and materials in a scene, enables the direct prediction of channel statistics. However, the process of frequently calibrating a DT to achieve this level of accuracy is resource-intensive, restricting its practical use to limited scenarios.

In contrast with prior works, this work presents a novel method that utilizes uncalibrated DTs generated from satellite images obtained from open-source maps, such as OpenStreetMap [7]. Rather than relying on a perfectly calibrated DT, the uncalibrated DT is employed to extract geometric features of the environment. These geometric features are combined with sparse channel measurements taken from a few anchor points to estimate the channel statistics across the entire scene. To enable this, we leverage the spatial interpolation capabilities of a Gaussian process (GP) along with the geometric consistency of the DT to predict channel statistics with high accuracy. Thus, by providing a geometry-informed GP framework for channel prediction, this work aims to improve the overall reliability and performance of wireless systems in a more efficient and scalable manner. The results show that the proposed geometry-informed GP significantly improves prediction accuracy across the entire scene compared to the benchmarks where (i) an uncalibrated DT directly predicts channel statistics and (ii) a GP uses location information to predict channel statistics. Moreover, when the channel statistics map is used in rate selection for URLLC, the proposed framework is shown to (approximately) double the data rate while maintaining the same reliability, compared to the benchmarks.

The paper is organized as follows. Sec. II describes the

This research is supported by the HORIZON JU-SNS-2022-STREAM-B-01-02 CENTRIC project (Grant Agreement No.101096379) and the Villum Investigator Grant “WATER” from the Velux Foundations, Denmark. Authors Mahmoud Saad Abouamer and Robin J. Williams contributed equally to this work

system model. Sec. III describes the scenario upon which the proposed framework is evaluated as well as the construction of the DT. Sec. IV describes the proposed methods for estimating the channel statistics map. Sec. V presents a range of simulation results based on the measured data. Finally, sec. VI concludes this paper.

Notation: i is the imaginary unit, $|\cdot|$ is the absolute value, vectors are denoted by bold lowercase symbols, $\mathbb{E}[x]$ is the expectation operator.

II. SYSTEM MODEL

This work considers a single receiver and a single transmitter, both equipped with a single antenna each. The transmitter is assumed to have access to an estimate of its location. The location of the receiver is static and known to all parties. Assuming an Orthogonal Frequency Division Multiplexing (OFDM) system, perfect clock synchronization, a channel without Doppler shifts, and delay-spread equalization, such as cyclic-prefixing, the signal received at the receiver at a given subcarrier is:

$$y = \sqrt{P_{\text{tx}}} h(\mathbf{x}) s + n \quad (1)$$

where $h(\mathbf{x}) \in \mathbb{C}$ is the frequency domain channel between the transmitter and receiver, $\mathbf{x} \in \mathbb{R}^{3 \times 1}$ is the transmitter location, $s \in \mathbb{C}$ is a random transmit symbol with mean $\mu_s = \mathbb{E}[s] = 0$ and variance $\sigma_s^2 = \mathbb{E}[ss^H] = 1$, $P_{\text{tx}} \in \mathbb{R}$ is the time-averaged transmit power, and $n \sim \mathcal{CN}(0, \sigma_n^2)$ is additive white Gaussian noise. The time-averaged signal to noise ratio is thus

$$\gamma(\mathbf{x}) = \mathbb{E} \left[\frac{|\sqrt{P_{\text{tx}}} h(\mathbf{x}) s|^2}{|n|^2} \right] = \frac{P_{\text{tx}} |h(\mathbf{x})|^2}{\sigma_n^2}. \quad (2)$$

The maximum rate that the channel can sustain under error-free communications is given through the channel capacity as [8]

$$R_{\text{max}} = B \cdot \log_2 (1 + \gamma(\mathbf{x})) \quad (3)$$

where B is the bandwidth of the subcarrier. Given known channel state information, the rate can thus be chosen in a straight forward manor as $R = R_{\text{max}}$. The channel coefficient, $h(\mathbf{x})$, is dependent on the propagation environment and it is commonly modeled as a realization of a random distribution. The randomness is in part due to imperfect channel estimation, dynamic changes of the environment, and inaccurate position estimation. The DT can be used to remove some of the uncertainty from $h(\mathbf{x})$, which, in effect, changes the distribution of $h(\mathbf{x})$ from the perspective of a system designer. The problem is then to find the maximum rate R for which the probability of *outage*, p_{out} , is less than ϵ ;

$$\begin{aligned} \epsilon > p_{\text{out}}(R) &= P(R_{\text{max}} < R), \\ &= P \left(B \cdot \log_2 \left(1 + \frac{P_{\text{tx}} |h(\mathbf{x})|^2}{\sigma_n^2} \right) < R \right), \\ \implies R < B \cdot \log_2 \left(1 + \frac{P_{\text{tx}} p_{\epsilon}(\mathbf{x})}{\sigma_n^2} \right) \end{aligned} \quad (4)$$

where $P(a < b)$ is the probability that $a < b$ and $p_{\epsilon}(\mathbf{x})$ is the ϵ -quantile the channel power which ideally can be obtained from the of the cumulative probability distribution of $p(\mathbf{x}) = |h(\mathbf{x})|^2$, given that the distribution of $h(\mathbf{x})$ is known. However, due to latency constants, just as the instantaneous value of $h(\mathbf{x})$ is unknown, so is the distribution of $h(\mathbf{x})$.

Assuming, similarly to [9], that the the logarithm of the ϵ -quantile channel power $q_{\epsilon}(\mathbf{x}) = \ln(p_{\epsilon}(\mathbf{x}))$ behaves as a multivariate Gaussian random variable across space, the power quantiles can be predicted over space through Gaussian process regression, given a set of known power quantiles. The estimation is done on the logarithm of the power quantiles as the logarithm provides a more Gaussian-like process. Consider the widely applied wide sense stationary uncorrelated scattering (WSSUS) channel model, in which the channel power, $p(\mathbf{x}) \sim \lambda(\mathbf{x}) e^{-\lambda(\mathbf{x})p} |p \geq 0$, follows an exponential distribution [10]. The natural logarithm of the channel power, $q(\mathbf{x}) = \ln(p(\mathbf{x})) \sim \lambda(\mathbf{x}) e^{q - \lambda(\mathbf{x})e^q}$, has a more Gaussian-like distribution and is thus better approximated by a multivariate Gaussian.

Obtaining spatial samples of the power quantiles, $p_{\epsilon}(\mathbf{x})$, necessary for ultra reliable communications, upon which to predict through Gaussian process regression, requires either relying on model based approaches which are susceptible to model mismatch errors, or a very high number of channel measurements to establish an empirical distribution, which results in high latency. An alternative approach proposed in [11] is to a range of subcarriers and use frequency as a proxy for space. By measuring a wide bandwidth, an empirical channel power distribution can be established and an estimate of the ϵ -quantile of the channel power, $p_{\epsilon}(\mathbf{x})$, can be extracted.

The validity of using frequency as a proxy for space can be argued by considering again the WSSUS Rayleigh fading channel [10]. In the farfield of the transmitter, the impinging field can be written as a position dependent distribution of planewaves. In quantizing the distribution, the received signal in the vicinity of a point \mathbf{x} can be written as

$$h(\mathbf{x}, f) \approx s \sum_{n=1}^N \alpha_n e^{-ik\mathbf{x}^T \mathbf{r}_n} e^{-i\tau_n f} \quad (5)$$

where $k \in \mathbb{R}$ is the wavenumber, $\mathbf{x} \in \mathbb{R}^{3 \times 1}$ is a point in the vicinity of \mathbf{x} and $\alpha_n \in \mathbb{C}$ is the amplitude and phase, $\mathbf{r}_n \in \{\mathbb{R}^{3 \times 1} | \mathbf{r}_n^T \mathbf{r}_n = 1\}$ is the normal, and τ_n is the excess delay of the n 'th planewave. In the Rayleigh channel, α_n is a set of zero mean independent identically distributed circular symmetric complex random variables. Independence between all τ_n , \mathbf{r}_n , and α_n is assumed. Due to α_n being circular symmetric complex random variables, $\mathbb{E}[h(\mathbf{x}, f)] = 0$. Additionally, due to the central limit theorem, $h(\mathbf{x}, f) \sim \mathcal{CN}(0, \sigma^2)$ for high N , where $\sigma^2 = \mathbb{E}[|h(\mathbf{x}, f)|^2]$. To allow relating the power quantile obtained from sampling across frequency to the power quantile obtained from sampling across space, the covariance properties of the channel across frequency and space,

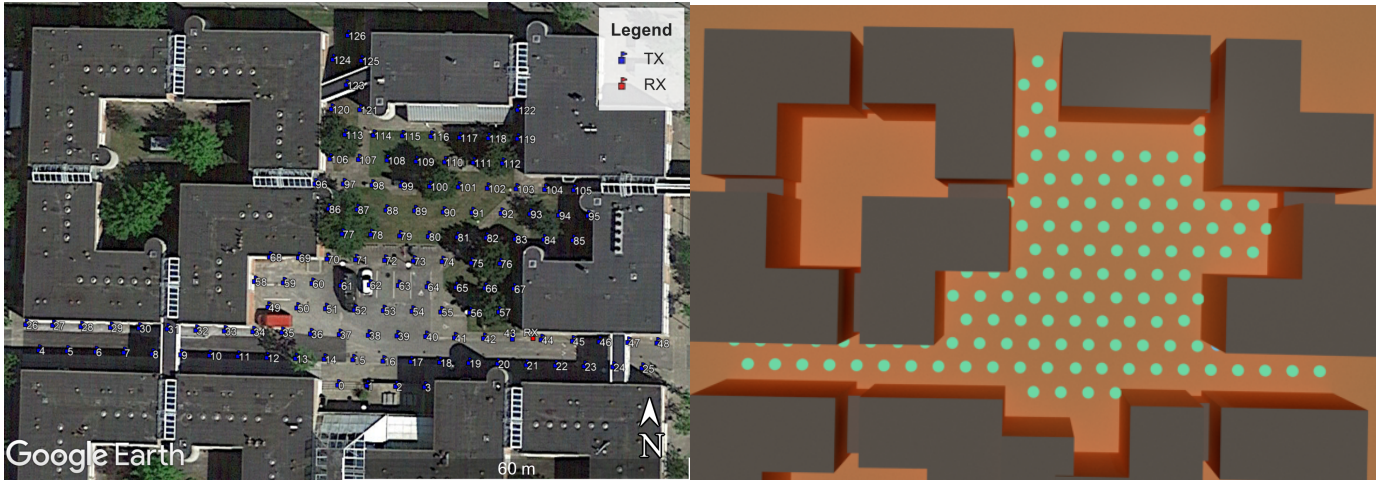


Fig. 1: Two pictures of the scenario. *Left*: A satellite picture of the outdoor scenario not taken at the day of the measurement. Transmitter locations marked with blue dots [11]. *Right*: Illustration of the geometry made using the `sionna.rt.scene.render` python library [12] and data extracted from OpenStreetMap [7]. Transmitter points are marked as green dots.

is analyzed. The channel covariance function is given as

$$\begin{aligned} \Sigma^2(\mathbf{x}_1, \mathbf{x}_2, f_1, f_2) &= \mathbb{E}[h(\mathbf{x}_1, f_1) h^*(\mathbf{x}_2, f_2)], \\ &= |s|^2 \sigma^2 c_{\mathbf{x}}(\mathbf{x}_1 - \mathbf{x}_2) c_f(f_1 - f_2), \end{aligned} \quad (6)$$

where $c_{\mathbf{x}}(\mathbf{x}) = \mathbb{E}[e^{-i\mathbf{k}\mathbf{x}^T \mathbf{r}_n}]$ is the spatial correlation function, and $c_f(f) = \mathbb{E}[e^{-i\tau_n f}]$ is the frequency correlation function. Assuming a uniform plane wave normal distribution, $\mathbf{r}_n = [\cos(\phi_n) \quad \sin(\phi_n) \quad 0]^T$ with $\phi_n \sim \mathcal{U}(0, 2\pi)$, as in Clarke's two-dimensional model [10, Sec. 5.4], and a uniform excess delay distribution $\tau_n \sim \mathcal{U}(0, \tau_{\max})$, the covariance functions are given as

$$c_{\mathbf{x}}(\mathbf{x}) = J_0\left(2\pi x \lambda^{-1}\right) \quad (7)$$

$$c_f(f) = \frac{1 - e^{-i\tau_{\max} f}}{i\tau_{\max} f} \quad (8)$$

where $x = \|\mathbf{x}\|_2$ is the distance and $\lambda \in \mathbb{R}$ is the wavelength. It can be observed that samples are approximately uncorrelated, $c_{\mathbf{x}}, c_f < 0.33$, for $x \geq 0.71\lambda$ and $f \geq 4.6\tau_{\max}^{-1}$. In setting $\tau_{\max} = 10dc^{-1}$ with c being the speed of light in a vacuum and d being the distance between transmitter and receiver, the channel is approximately uncorrelated for a frequency shift of $f = 1.4$ MHz at a distance of 100 m, and approximately uncorrelated for a frequency shift of $f = 6.9$ MHz at a distance of 20 m. Thus, given sufficient bandwidth and distance, sampling across frequency and space is equivalent of drawing independent random samples from the same distribution. The usage of frequency as a proxy for space, is further verified through the DT in Sec. III.

III. SCENARIO

Evaluation of the proposed system is done using the data from the measurement campaign described in [11]. The data consists of wideband channel measurements done with a

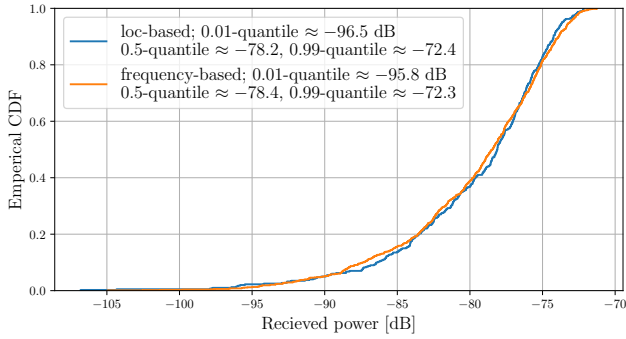
stationary receiver and 127 different transmitter locations. Both the transmitter and receiver are equipped with omnidirectional antennas. The layout of the measurement campaign is illustrated on Fig. 1 *Left*. The layout of the digital twin of the same scenario is illustrated on Fig. 1 *Right*, with the digital-twin (DT) equivalent 127 transmitter locations marked as green dots. At each of the 127 locations, 8001 equispaced frequency domain channel measurements are made, spanning the bandwidth from 2 GHz to 10 GHz, yielding a frequency resolution of 1 MHz. The geometry used in the digital twin is extracted from OpenStreetMap [7] using the *Blosm for Blender* blender plugin and imported into the *sionna* python library [12]. All surfaces, ground included, are assigned the *sionna*-defined `itu_brick` material which has a relative permittivity of $\epsilon_r = 3.91$ [13, table 3].

A. Approximating the statistics of small-scale fading via frequency-domain sampling

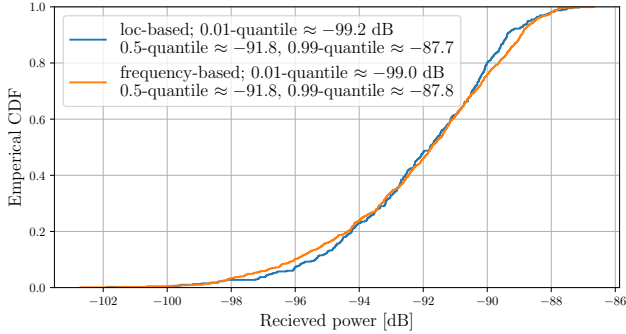
In Sec. II and [11], it was argued the small-scale fading distribution, that results from small changes in location, can be approximated using the wideband frequency-domain channel power distribution.

We verify this claim using the geometry-consistent DT of the scene. For each of the 127 transmitter locations, the small-scale fading distribution is computed by generating a grid of 400 small movements (on the order of a wavelength λ) in the transmitter's x and y coordinates. Using the channel impulse response (CIR) generated by the DT, an empirical *location-based* distribution of the channel power in dB is computed. The empirical *frequency-based* channel power distribution is obtained by fixing the transmitter's position and sampling the frequency domain over a large bandwidth (i.e., 8 GHz, as suggested by [11]).

Fig. 2 shows the empirical cumulative distribution functions (CDFs) of received power for both the frequency-based and



(a) Near the transmitter



(b) Far from the transmitter

Fig. 2: Frequency based and location based CDF of received power (left) near transmitter and (right) far from the transmitter.

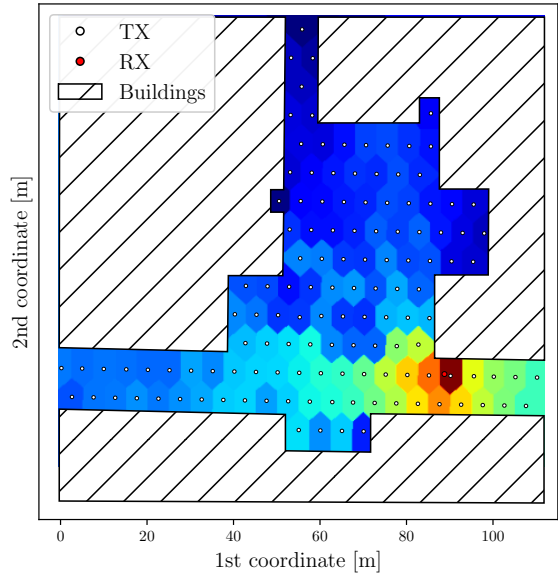
location-based approaches. The results are shown for two typical transmitter positions (a) near the transmitter (position 55 in Fig. 1) and (b) far from the transmitter (position 111 in Fig. 1). As Fig. 2 shows, the frequency-domain channel power distribution closely approximates the location-based channel power distribution, including the tails of the distributions. For example, when the receiver is far from the transmitter, the 0.01-quantiles of the location-based and frequency-based distributions differ by only 0.02 dB. Thus, frequency-domain samples, which can be obtained by wideband channel sounding, offers a practical method to approximate small-scale fading distributions that are otherwise challenging to capture directly [11].

IV. SITE-SPECIFIC CHANNEL STATISTICS PREDICTION

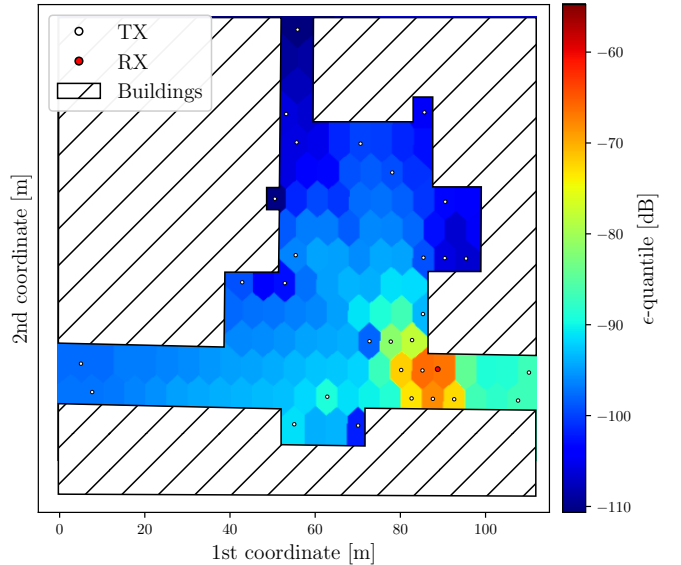
For the scenario considered in Fig. 1, let $p(\mathbf{x})$ indicate the instantaneous received power associated a transmitter located at position \mathbf{x} . Due to small scale fading, $p(\mathbf{x})$ is modeled as a random variable. As demonstrated in [11], reliable rate selection can be achieved using accurate estimates of the statistics of $p(\mathbf{x})$. Particularly, The goal is to estimate the log ϵ -quantile $q_\epsilon(\mathbf{x})$

$$\begin{aligned} \rho_\epsilon(\mathbf{x}) &= \sup\{\rho > 0 | P(p(\mathbf{x}) \leq \rho) < \epsilon\} \\ q_\epsilon(\mathbf{x}) &= \ln(\rho_\epsilon(\mathbf{x})) \end{aligned} \quad (9)$$

For each position \mathbf{x} , a DT can ideally be used to estimate the CDF of the received power $\psi^{\text{DT}}(\beta, \mathbf{x}) = P(p(\mathbf{x}) \leq \beta)$



(a) Ground truth



(b) Prediction by proposed GP

Fig. 3: Closest point interpolation of ϵ -quantile of fading in dB associated with (ground truth) measurements and predictions by proposed GP and $D = 30$ observations.

which can then be directly used to provide an estimate $q_\epsilon^{\text{direct}}(\mathbf{x})$. However, in this work, we consider *uncalibrated* DTs generated from open-source maps (e.g. OpenStreetMap [7]) and with default material properties. Thus, due to mismatched material properties, changes in the wireless environment and other non-idealities, the direct use of a DT does not necessarily provide an accurate estimate of $q_\epsilon(\mathbf{x})$. However, the DT's received power CDF $\psi^{\text{DT}}(\beta, \mathbf{x})$ can be leveraged to provide site-specific geometric insights. We propose to exploit the geometric information implicitly conveyed by $\psi^{\text{DT}}(\cdot)$ and a small number of channel measurements to predict fading statistics across the entire site.

Let $\mathcal{D} = \{\mathbf{x}_d, q_\epsilon(\mathbf{x}_d)\}_{d=1}^D$ be a data set of log-fading power quantiles formed using D measurements. The quantile function $q_\epsilon(\mathbf{x})$ is modeled as GP. As demonstrated in [11], GP regression can be used to predict fading statistics by spatially interpolating channel measurements using a predictive distribution

$$q_\epsilon^{\text{spatial}}(\mathbf{x}|\mathcal{D}) \sim \mathcal{N}(\mu(\mathbf{x}|\mathcal{D}), \sigma^2(\mathbf{x}|\mathcal{D})). \quad (10)$$

In this work, instead of relying on spatial features alone, we employ GP regression to predict fading statistics using geometric features derived from the DT. In particular, by processing the DT's distribution of received power $\psi^{\text{DT}}(\beta, \mathbf{x})$, we employ a predictive distribution

$$q_\epsilon^{\text{DT}}(\mathbf{x}|\mathcal{D}) \sim \mathcal{N}(\mu_{\text{DT}}(\mathbf{y}|\mathcal{D}), \sigma_{\text{DT}}^2(\mathbf{y}|\mathcal{D})), \quad (11)$$

$$\mathbf{y} = (\mathbf{x}, \mathbf{f}(\psi^{\text{DT}}(\beta, \mathbf{x}))). \quad (12)$$

Here $\mathbf{f}(\cdot)$ uniformly samples 100 points from the DT's CDF of received power $\psi^{\text{DT}}(\beta, \mathbf{x})$. With this \mathbf{y} and the use of an anisotropic GP kernel $k(\mathbf{y}, \mathbf{y}')$, the GP does not only capture spatial similarities but also implicitly encodes geometric information provided by the DT. Particularly, for two receiver positions \mathbf{x}_1 and \mathbf{x}_2 that result in similar DT outputs $\psi^{\text{DT}}(\beta, \mathbf{x}_1) \approx \psi^{\text{DT}}(\beta, \mathbf{x}_2)$, the GP's covariance function ensures that the predicted channel statistics at these two locations are close to each other. Thus, the DT's geometric features are captured via the GP's covariance function, embedding geometric correlations that allows efficient prediction of channel statistics using a limited number of measurements.

In Section V, using a measurement campaign conducted in the site shown in Fig. 1, we corroborate the effectiveness of the proposed $q_\epsilon^{\text{DT}}(\mathbf{x}|\mathcal{D})$ in predicting channel statistics with high accuracy. Moreover, this proposed prediction framework is shown to provide significant improvements in prediction errors compared to the following *benchmarks*:

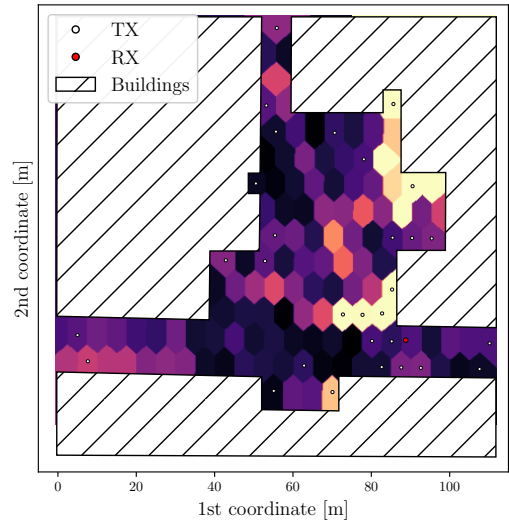
- *benchmark 1*: direct prediction scheme using $q_\epsilon^{\text{direct}}(\mathbf{x})$.
- *benchmark 2*: spatial prediction scheme $q_\epsilon^{\text{spatial}}(\mathbf{x}|\mathcal{D})$.

V. NUMERICAL RESULTS

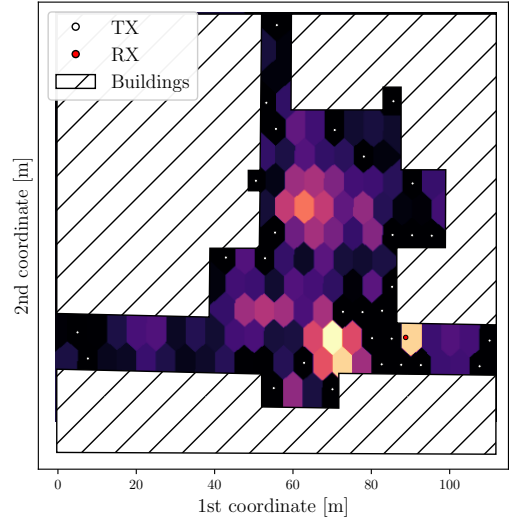
A. Channel Statistics Predictions

In this section, we consider $\epsilon = 1\%$ and the measurement campaign data associated with the setup in Fig 1 which is split into a (small) training set and an evaluation set. Here, the (training) data set is given $\mathcal{D} = \{\mathbf{x}_d, q_\epsilon(\mathbf{x}_d)\}_{d=1}^D$ with $D = 30$. The goal is to predict the ϵ -quantile associated with the remaining $127 - 30$ positions.

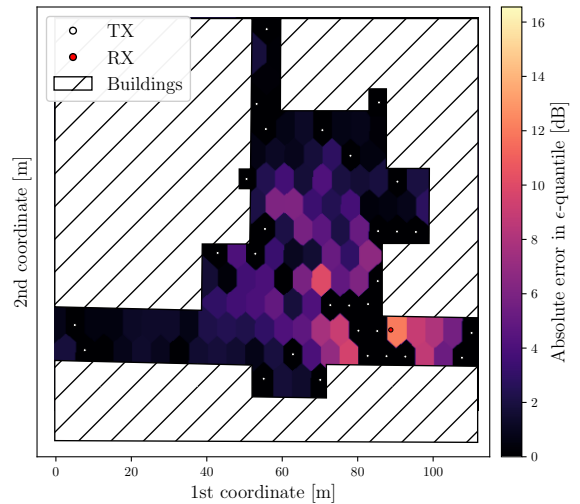
We demonstrate the ability of the proposed prediction framework $q_\epsilon^{\text{DT}}(\mathbf{x}|\mathcal{D}) \sim \mathcal{N}(\mu_{\text{DT}}(\mathbf{y}|\mathcal{D}), \sigma_{\text{DT}}^2(\mathbf{y}|\mathcal{D}))$ presented in Section IV. Fig. (3a) shows ϵ -quantile of fading under the ground-truth measurements obtained through closest point interpolation. Fig. (3b) shows $\mu_{\text{DT}}(\mathbf{y}|\mathcal{D})$ used to predict ϵ -quantile of fading with \mathcal{D} containing 30 observations (corresponding locations are indicated with white dots). To quantify estimation errors, compared to ground-truth measurements in Fig. (3a), Fig. (4c) shows the absolute prediction error incurred by $\mu_{\text{DT}}(\mathbf{y}|\mathcal{D})$. For comparison, Fig. (4a) and Fig. (4b) show the absolute prediction error incurred by the two benchmarks



(a) Prediction errors by (uncalibrated) DT



(b) Prediction errors by baseline GP



(c) Prediction errors by proposed GP with DT features

Fig. 4: Absolute Error in predicting ϵ -quantile of fading using DT, GP baseline and Proposed GP.

described in Section IV: (a) directly using DT for prediction $q_\epsilon^{\text{direct}}(\mathbf{x})$ and (b) using spatial features only $q_\epsilon^{\text{spatial}}(\mathbf{x}|\mathcal{D})$. As shown in the figure, compared to the benchmarks, the proposed method significantly improves prediction accuracy across the entire scene by effectively leveraging the geometric consistency of the DT. For instance, the proposed prediction scheme reduces the median error to 1.8 dB compared to 3.7 dB and 3.2 dB associated with $q_\epsilon^{\text{direct}}(\mathbf{x})$ and $q_\epsilon^{\text{spatial}}(\mathbf{x}|\mathcal{D})$, respectively.

As we will demonstrate next, this improvement in channel statistics prediction can significantly enhance the reliability and performance of a wireless systems.

B. Rate selection under reliability constraints

For a position \mathbf{x} , the predictive distribution $q_\epsilon^{\text{DT}}(\mathbf{x}|\mathcal{D})$ is employed to select a rate $R^{\text{DT}}(\mathbf{x}|\mathcal{D})$ that complies with a meta-probability $\tilde{p}_\epsilon(\mathbf{x})$ reliability constraint [9]. In particular, for a confidence parameter $\delta > 0$, the goal is to select $R^{\text{DT}}(\mathbf{x}|\mathcal{D})$ such that the corresponding meta-probability $\tilde{p}_\epsilon^{\text{DT}}(\mathbf{x}) \leq \delta$. Following [11], $R^{\text{DT}}(\mathbf{x}|\mathcal{D})$ is selected using the predictive distribution $q_\epsilon^{\text{DT}}(\mathbf{x}|\mathcal{D})$ given in (11). Here, the rate is selected as the δ -quantile of $q_\epsilon^{\text{DT}}(\mathbf{x}|\mathcal{D})$. In particular, for predictive mean $\mu_{\text{DT}}(\mathbf{y}|\mathcal{D})$ and predictive variance $\sigma_{\text{DT}}^2(\mathbf{y}|\mathcal{D})$,

$$R^{\text{DT}}(\mathbf{x}|\mathcal{D}) = \log_2 \left(1 + e^{\mu_{\text{DT}}(\mathbf{y}|\mathcal{D}) + \sqrt{2}\sigma_{\text{DT}}(\mathbf{y}|\mathcal{D}) \text{erf}^{-1}(2\delta-1)} \right). \quad (13)$$

The predictive distribution $q_\epsilon^{\text{spatial}}(\mathbf{x}|\mathcal{D}) \sim \mathcal{N}(\mu(\mathbf{x}|\mathcal{D}), \sigma^2(\mathbf{x}|\mathcal{D}))$ can be similarly used to select a corresponding rate $R^{\text{spatial}}(\mathbf{x}|\mathcal{D})$.

To evaluate the performance of $R^{\text{DT}}(\mathbf{x}|\mathcal{D})$, we compute its ratio with respect to the ϵ -outage capacity $R_\epsilon(\mathbf{x})$ computed using the (perfect channel knowledge) ground truth fading distribution. This metric is referred to the *normalized rate* and is given by

$$\hat{R}_\epsilon^{\text{DT}}(\mathbf{x}) = \frac{R^{\text{DT}}(\mathbf{x}|\mathcal{D})}{R_\epsilon(\mathbf{x})}. \quad (14)$$

For $\epsilon = 1\%$ and $\delta = 10\%$, Fig. (5) shows the CDF of $R_\epsilon^{\text{DT}}(\mathbf{x})$ across the 127–30 (testing) locations. For comparison, Fig. (5) also shows the normalized rate $\hat{R}_\epsilon^{\text{spatial}}(\mathbf{x}) = R^{\text{spatial}}(\mathbf{x}|\mathcal{D})/R_\epsilon(\mathbf{x})$. As shown in Fig. (5), both $R^{\text{DT}}(\mathbf{x}|\mathcal{D})$ and $R^{\text{spatial}}(\mathbf{x}|\mathcal{D})$ meet the meta-probability reliability criteria. However, the proposed $R^{\text{DT}}(\mathbf{x}|\mathcal{D})$ provides significant boost in the selected rate compared to $R^{\text{spatial}}(\mathbf{x}|\mathcal{D})$ and as shown by the shift in normalized rate in Fig. (5). For instance, across different locations, the average normalized rate is approximately doubled from $\hat{R}_\epsilon^{\text{spatial}}(\mathbf{x}) = 0.27$ from to $\hat{R}_\epsilon^{\text{DT}}(\mathbf{x}) = 0.45$. Thus, compared to $q_\epsilon^{\text{spatial}}(\mathbf{x}|\mathcal{D})$, $q_\epsilon^{\text{DT}}(\mathbf{x}|\mathcal{D})$ allows selection of higher rates while complying with reliability constraints.

VI. CONCLUSIONS

In this paper we have shown that by incorporating raytraced channel information from an inaccurate DT, one can improve the accuracy of channel statistics prediction. The proposed system is capable of almost doubling the provided data rate while maintaining the same reliability, when compared with

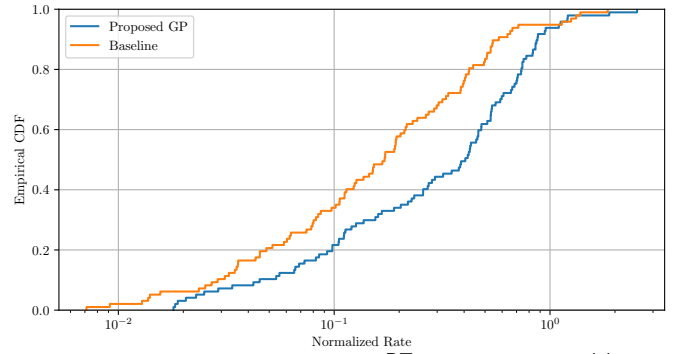


Fig. 5: Empirical distribution of $R^{\text{DT}}(\mathbf{x}|\mathcal{D})$ and $R^{\text{spatial}}(\mathbf{x}|\mathcal{D})$ normalized by ϵ -outage capacity $R_\epsilon(\mathbf{x})$ for $\epsilon = 1\%$ and $\delta = 10\%$.

the baseline. This increase does not come at the expense of increased overhead and lengthy DT calibration procedures, as the system utilizes an uncalibrated DT based on geometry from OpenStreetMap [7] with all objects, ground included, having material parameters equal to that of a brick wall. The proposed framework successfully utilizes a DT based on freely available geometry data without calibration to directly improve the performance of a communication system.

REFERENCES

- [1] N. P. Kuruvatti, M. A. Habibi, S. Partani, B. Han, A. Fellan, and H. D. Schotten, "Empowering 6g communication systems with digital twin technology: A comprehensive survey," *IEEE Access*, vol. 10, pp. 112 158–112 186, 2022.
- [2] S. Jiang and A. Alkhateeb, "Digital Twin Aided Massive MIMO: CSI Compression and Feedback," in *ICC 2024*. Denver, CO, USA: IEEE, Jun. 2024, pp. 3586–3591.
- [3] J. Morais and A. Alkhateeb, "Localization in Digital Twin MIMO Networks: A Case for Massive Fingerprinting," in *ICC Workshops 2024*. Denver, CO, USA: IEEE, Jun. 2024, pp. 276–281.
- [4] J. Hoydis, F. A. Aoudia, S. Cammerer, M. Nimier-David, N. Binder, G. Marcus, and A. Keller, "Sionna rt: Differentiable ray tracing for radio propagation modeling," in *Globecom Workshops 2023*. IEEE, 2023, pp. 317–321.
- [5] J. Hoydis, F. A. Aoudia, S. Cammerer, F. Euchner, M. Nimier-David, S. T. Brink, and A. Keller, "Learning radio environments by differentiable ray tracing," *IEEE Transactions on Machine Learning in Communications and Networking*, vol. 2, pp. 1527–1539, 2024.
- [6] C. Ruah, O. Simeone, J. Hoydis, and B. Al-Hashimi, "Calibrating wireless ray tracing for digital twinning using local phase error estimates," *IEEE Transactions on Machine Learning in Communications and Networking*, vol. 2, pp. 1193–1215, 2024.
- [7] "OpenStreetMap," <https://www.openstreetmap.org>, accessed: 2024.
- [8] W. Yang, G. Durisi, T. Koch, and Y. Polyanskiy, "Quasi-Static Multiple-Antenna Fading Channels at Finite Blocklength," *IEEE Transactions on Information Theory*, vol. 60, no. 7, pp. 4232–4265, Jul. 2014.
- [9] T. Kallehauge, P. Ramírez-Espinosa, A. E. Kalør, C. Biscio, and P. Popovski, "Predictive rate selection for ultra-reliable communication using statistical radio maps," in *GLOBECOM 2022*. IEEE, 2022, pp. 4989–4994.
- [10] J. D. Parsons, *The mobile radio propagation channel*, 2nd ed. Chichester : New York: J. Wiley, 2000.
- [11] T. Kallehauge, A. E. Kalør, F. Zhang, and P. Popovski, "Experimental Study of Spatial Statistics for Ultra-Reliable Communications," in *ICC 2024*. Denver, CO, USA: IEEE, Jun. 2024, pp. 629–634.
- [12] J. Hoydis, S. Cammerer, F. Ait Aoudia, A. Vem, N. Binder, G. Marcus, and A. Keller, "Sionna: An open-source library for next-generation physical layer research," *arXiv preprint*, Mar. 2022.
- [13] "Recommendation ITU-R P.2040-3 (08/2023) - Effects of building materials and structures on radiowave propagation above about 100 MHz."